A New Fifth Order Finite Difference WENO Scheme for Hamilton-Jacobi Equations

Jun Zhu,[1] **Jianxian Qiu**[2]

[1] *College of Science, Nanjing University of Aeronautics and Astronautics, Nanjing, Jiangsu 210016, People's Republic of China*

[2] *School of Mathematical Sciences and Fujian Provincial Key Laboratory of Mathematical Modeling and High-Performance Scientific Computing, Xiamen University, Xiamen, Fujian 361005, People's Republic of China*

Received 2 June 2016; revised 27 November 2016; accepted 15 December 2016
Published online 3 February 2017 in Wiley Online Library (wileyonlinelibrary.com).
DOI 10.1002/num.22133

In this continuing paper of (Zhu and Qiu, J Comput Phys 318 (2016), 110–121), a new fifth order finite difference weighted essentially non-oscillatory (WENO) scheme is designed to approximate the viscosity numerical solution of the Hamilton-Jacobi equations. This new WENO scheme uses the same numbers of spatial nodes as the classical fifth order WENO scheme which is proposed by Jiang and Peng (SIAM J Sci Comput 21 (2000), 2126–2143), and could get less absolute truncation errors and obtain the same order of accuracy in smooth region simultaneously avoiding spurious oscillations nearby discontinuities. Such new WENO scheme is a convex combination of a fourth degree accurate polynomial and two linear polynomials in a WENO type fashion in the spatial reconstruction procedures. The linear weights of three polynomials are artificially set to be any random positive constants with a minor restriction and the new nonlinear weights are proposed for the sake of keeping the accuracy of the scheme in smooth region, avoiding spurious oscillations and keeping sharp discontinuous transitions in nonsmooth region simultaneously. The main advantages of such new WENO scheme comparing with the classical WENO scheme proposed by Jiang and Peng (SIAM J Sci Comput 21 (2000), 2126–2143) are its efficiency, robustness and easy implementation to higher dimensions. Extensive numerical tests are performed to illustrate the capability of the new fifth WENO scheme.

Keywords: finite difference framework; Hamilton-Jacobi equation; weighted essentially non-oscillatory scheme

Correspondence to: Jianxian Qiu, School of Mathematical Sciences and Fujian Provincial Key Laboratory of Mathematical Modeling and High-Performance Scientific Computing, Xiamen University, Xiamen, Fujian 361005, People's Republic of China (e-mail: jxqiu@xmu.edu.cn)
Contract grant sponsor: NSFC (J. Zhu); contract grant number: 11372005
Contract grant sponsor: State Scholarship Fund of China for studying abroad (J. Zhu)
Contract grant sponsor: NSFC (J. Qiu); contract grant number: 11571290
Contract grant sponsor: NSAF (J. Qiu); contract grant number: U1630247

I. INTRODUCTION

In this paper, we present a new fifth-order accurate finite difference weighted essentially non-oscillatory (WENO) reconstruction methodology for solving the Hamilton-Jacobi (H-J) equations:

$$\begin{cases} \phi_t + H(x_1, \cdots, x_n, t, \phi, \nabla\phi) = 0, & (x_1, \ldots, x_n, t) \in \Omega \times [0, \infty), \\ \phi(x_1, \ldots, x_n, 0) = \phi_0(x_1, \ldots, x_n), & (x_1, \ldots, x_n) \in \Omega, \end{cases} \tag{1.1}$$

where $\nabla\phi = (\phi_{x_1}, \ldots, \phi_{x_n})^T$. The Hamilton-Jacobi equations are often used in many applications such as geometric optics, computer vision, material science, image processing and variational calculus [1–3] and so on. It is well known that the solutions to (1.1) are continuous but their associated derivatives might be discontinuous. And such solutions may not be unique unless using the physical implications and then getting the viscosity solutions [4]. As everyone knows, the H-J equations are closely related to conservation laws, hence we can get the exact solutions of H-J equations from those of conservation laws and successful numerical methods for conservation laws can be adapted for solving the H-J equations. In this literature, we refer the crucial works, Osher and Sethian [5] presented a second order essentially non-oscillatory (ENO) scheme and Osher and Shu [6] put forward some high order ENO schemes for solving the Hamilton-Jacobi equations. In 2000, a finite difference fifth-order accurate weighted ENO (WENO) scheme was proposed by Jiang and Peng [7]. Recently, Qiu [8, 9] and together with Shu [10] also gained Hermite WENO schemes for solving the Hamilton-Jacobi equations on structured meshes. In 1996, Lafon and Osher [11] constructed the ENO schemes for solving the Hamilton-Jacobi equations on unstructured meshes. Recently, Zhang and Shu [12], Li and Chan [13] investigated high order WENO schemes for solving two-dimensional Hamilton-Jacobi equations by the usage of the nodal based WENO polynomial reconstructions on triangular meshes. And some finite element methods for arbitrary triangular meshes were proposed in [14–17]. In 1999, Hu and Shu [16] applied a discontinuous Galerkin (DG) framework on the conservation law system satisfied by the derivatives of the solution to solve H-J equations. Based on such DG method, in 2007, Cheng and Shu presented direct DG methods to solve for the H-J equations (1.1) for ϕ in [18] and new flux was presented to keep stability of the method. In [19], Yan and Osher gave a new DG method to directly solve H-J Eq. (1.1), in which a local DG method was applied to approximate derivatives of ϕ precisely.

Following the original idea of WENO methodologies [20, 21], this paper is mainly based on [7] and is a new generation of the approach of doing WENO in [22] from conservation laws to Hamilton-Jacobi equations in the literature. Comparing with the classical WENO schemes of Jiang and Peng [7], the major advantage of this new fifth order WENO scheme is its easy implementation in the computation. This new WENO scheme has a convex combination of a modified fourth degree polynomial which should subtract other two linear polynomials by multiplying proper constant parameters first, then compound these three unequal degree polynomials in a WENO type methodology including artificially setting linear weights for the robustness, computing smoothness indicators and proposing a new type of nonlinear weights which are little different from the formula specified in [22–24], for solving the Hamilton-Jacobi equations in one and two dimensions. The essential merits of such methodology are its robustness in spatial field by the definition of positive linear weights, and only one six-point stencil and two three-point stencils are used to reconstruct three different polynomials. The thought to modify the fourth degree polynomial is very crucial for obtaining the scheme's high-order accuracy, otherwise, the traditional WENO methodology will inevitably degrade its numerical accuracy. Therefore, we try to use central scheme in smooth regions for simplicity and easy implementation for the

sake of obtaining high-order accuracy, and switch it to either of two second order schemes on compact spatial stencils when the computing field is adjacent discontinuities for the purpose of avoiding spurious oscillations. Thereafter, new nonlinear weight formulas are presented for these polynomials of different degrees based on the information defined on the unequal size stencils [25, 26]. Generally speaking, the primary innovations of this paper lie in three aspects: the new way of reconstructing the modified fourth degree polynomial by subtracts two linear polynomials with different parameters, a robust WENO type communications among three unequal (modified) polynomials for high accurate approximations to the derivative quantities in different directions and the new manner of obtaining associated nonlinear weights.

The organization of this paper is as follows: In Section II, we review and construct the new fifth-order accurate finite difference WENO scheme in 1D and 2D in detail for solving the Hamilton-Jacobi equations and present extensive numerical results in Section III to verify the accuracy and easy implementation of these approaches. Concluding remarks are given in Section IV.

II. NEW WENO SCHEME FOR HAMILTON-JACOBI EQUATION

In this section, we give the framework for solving the Hamilton-Jacobi equations briefly and then develop the procedures of the new WENO scheme for both one and two-dimensional Hamilton-Jacobi equations in detail.

A. The framework for one-dimensional case

We take the control Eq. (1.1) in one dimension. For simplicity, the computational field Ω has been divided as the uniform mesh with intervals $I_i = [x_{i-1/2}, x_{i+1/2}], \quad i = 1, \ldots, N$. We denote $x_i = \frac{1}{2}(x_{i-1/2} + x_{i+1/2})$ to be the interval center and $|I_i| = h$ to be the length of I_i, respectively. (1.1) can be rewritten in one dimension as:

$$\begin{cases} \phi_t + H(x, t, \phi, \phi_x) = 0, \\ \phi(x, 0) = \phi_0(x). \end{cases} \tag{2.1}$$

We define $\phi_i \equiv \phi_i(t) = \phi(x_i, t)$ and $\triangle^+ \phi_i = \phi_{i+1} - \phi_i$. And we would like to omit variable t in the following if not cause confusion. The semidiscrete form is

$$\frac{d\phi_i(t)}{dt} = L(\phi_i) = -\hat{H}(x_i, t, \phi_i, \phi^+_{x,i}, \phi^-_{x,i}). \tag{2.2}$$

Where $\hat{H}$ is a Lipschitz continuous monotone flux consistent with H, in the sense that $\hat{H}(x, t, \phi, \phi_x, \phi_x) = H(x, t, \phi, \phi_x)$. The Lax-Friedrichs flux is applied here:

$$\hat{H}(x, t, \phi, u^+, u^-) = H\left(x, t, \phi, \frac{u^+ + u^-}{2}\right) - \alpha \frac{u^+ - u^-}{2}, \tag{2.3}$$

where $\alpha = \max_u |H_1(u)|$. And H_1 stands for the partial derivative of H with respect to ϕ_x.

Now, we would like to reconstruct the approximations of $\phi_{x,i}$ from the left and right sides of the point x_i, and these procedures confirm the new scheme's high order of accuracy in smooth regions. The simple flowchart is elaborated in detail as follows:

Step 1. For the purpose of approximating $\phi_x(x_i)$ on a left-biased six-point stencil $\{x_{i-3}, \ldots, x_{i+2}\}$ and on a right-biased six-point stencil $\{x_{i-2}, \ldots, x_{i+3}\}$, we do some definitions of the polynomials as:

$p_1^-(x)$ is a fourth degree polynomial defined on $\{x_{i-3}, x_{i-2}, x_{i-1}, x_i, x_{i+1}, x_{i+2}\}$ and satisfies

$$\frac{1}{h}\int_{x_j}^{x_{j+1}} p_1^-(x)dx = \frac{\triangle^+\phi_j}{h},\ j = i-3, i-2, i-1, i, i+1. \tag{2.4}$$

$p_1^+(x)$ is a fourth degree polynomial defined on $\{x_{i-2}, x_{i-1}, x_i, x_{i+1}, x_{i+2}, x_{i+3}\}$ and satisfies

$$\frac{1}{h}\int_{x_j}^{x_{j+1}} p_1^+(x)dx = \frac{\triangle^+\phi_j}{h},\ j = i-2, i-1, i, i+1, i+2. \tag{2.5}$$

$p_2^-(x)$ is a linear polynomial defined on $\{x_{i-2}, x_{i-1}, x_i\}$ and satisfies

$$\frac{1}{h}\int_{x_j}^{x_{j+1}} p_2^-(x)dx = \frac{\triangle^+\phi_j}{h},\ j = i-2, i-1. \tag{2.6}$$

$p_2^+(x)$ is a linear polynomial defined on $\{x_{i-1}, x_i, x_{i+1}\}$ and satisfies

$$\frac{1}{h}\int_{x_j}^{x_{j+1}} p_2^+(x)dx = \frac{\triangle^+\phi_j}{h},\ j = i-1, i. \tag{2.7}$$

$p_3^-(x)$ is a linear polynomial defined on $\{x_{i-1}, x_i, x_{i+1}\}$ and satisfies

$$\frac{1}{h}\int_{x_j}^{x_{j+1}} p_3^-(x)dx = \frac{\triangle^+\phi_j}{h},\ j = i-1, i. \tag{2.8}$$

$p_3^+(x)$ is a linear polynomial defined on $\{x_i, x_{i+1}, x_{i+2}\}$ and satisfies

$$\frac{1}{h}\int_{x_j}^{x_{j+1}} p_3^+(x)dx = \frac{\triangle^+\phi_j}{h},\ j = i, i+1. \tag{2.9}$$

The fifth order approximations of ϕ_x at x_i from left and right sides are given, respectively, by

$$\begin{aligned}\phi_{x,i}^{-,1} &= p_1^-(x_i) = \\ &+ \frac{1}{30}\frac{\triangle^+\phi_{i-3}}{h} - \frac{13}{60}\frac{\triangle^+\phi_{i-2}}{h} + \frac{47}{60}\frac{\triangle^+\phi_{i-1}}{h} + \frac{9}{20}\frac{\triangle^+\phi_i}{h} - \frac{1}{20}\frac{\triangle^+\phi_{i+1}}{h},\end{aligned} \tag{2.10}$$

$$\begin{aligned}\phi_{x,i}^{+,1} &= p_1^+(x_i) = \\ &- \frac{1}{20}\frac{\triangle^+\phi_{i-2}}{h} + \frac{9}{20}\frac{\triangle^+\phi_{i-1}}{h} + \frac{47}{60}\frac{\triangle^+\phi_i}{h} - \frac{13}{60}\frac{\triangle^+\phi_{i+1}}{h} + \frac{1}{30}\frac{\triangle^+\phi_{i+2}}{h},\end{aligned} \tag{2.11}$$

the the third order approximations of ϕ_x at x_i from left and right sides are given, respectively, by

$$\phi_{x,i}^{-,2} = p_2^-(x_i) = -\frac{1}{2}\frac{\triangle^+\phi_{i-2}}{h} + \frac{3}{2}\frac{\triangle^+\phi_{i-1}}{h}, \tag{2.12}$$

$$\phi_{x,i}^{+,2} = p_2^+(x_i) = \frac{1}{2}\frac{\triangle^+\phi_{i-1}}{h} + \frac{1}{2}\frac{\triangle^+\phi_i}{h}, \tag{2.13}$$

$$\phi_{x,i}^{-,3} = p_3^-(x_i) = \frac{1}{2}\frac{\triangle^+\phi_{i-1}}{h} + \frac{1}{2}\frac{\triangle^+\phi_i}{h}, \tag{2.14}$$

$$\phi_{x,i}^{+,3} = p_3^+(x_i) = \frac{3}{2}\frac{\triangle^+\phi_i}{h} - \frac{1}{2}\frac{\triangle^+\phi_{i+1}}{h}, \tag{2.15}$$

Step 2. Set any positive linear weights $\gamma_1, \gamma_2, \gamma_3$, such that $\gamma_1 + \gamma_2 + \gamma_3 = 1$, in this paper, we take $\gamma_1 = 0.998$ and $\gamma_2 = \gamma_3 = 0.001$.

Step 3. Compute the smoothness indicators $\beta_n^{\pm}$, which measure how smooth the functions $p_n^{\pm}(x)$ are in the target cells $[x_{i-1}, x_i]$ and $[x_i, x_{i+1}]$, respectively. The smaller these smoothness indicators, the smoother the functions are in different target cells. We use the similar recipe for the smoothness indicators as in [27, 28].

$$\beta_n^- = \sum_{\alpha=1}^{r}\int_{x_i-1}^{x_i} h^{2\alpha-1}\left(\frac{d^\alpha p_n^-(x)}{dx^\alpha}\right)^2 dx, n = 1, 2, 3, \tag{2.16}$$

and

$$\beta_n^+ = \sum_{\alpha=1}^{r}\int_{x_i}^{x_{i+1}} h^{2\alpha-1}\left(\frac{d^\alpha p_n^+(x)}{dx^\alpha}\right)^2 dx, n = 1, 2, 3. \tag{2.17}$$

For $n = 1$, r equals four and if $n = 2$, 3, r equals one. The associated smoothness indicators are explicitly written and the associated expansions of them in Taylor series about ϕ_i are obtained as

$$\begin{aligned}
\beta_1^- &= \frac{1}{144}\left(\frac{\triangle^+\phi_{i-3}}{h} - 8\frac{\triangle^+\phi_{i-2}}{h} + 8\frac{\triangle^+\phi_i}{h} - \frac{\triangle^+\phi_{i+1}}{h}\right)^2 \\
&\quad + \frac{1}{15600}\left(-11\frac{\triangle^+\phi_{i-3}}{h} + 174\frac{\triangle^+\phi_{i-2}}{h} - 326\frac{\triangle^+\phi_{i-1}}{h} + 174\frac{\triangle^+\phi_i}{h} - 11\frac{\triangle^+\phi_{i+1}}{h}\right)^2 \\
&\quad + \frac{781}{2880}\left(-\frac{\triangle^+\phi_{i-3}}{h} + 2\frac{\triangle^+\phi_{i-2}}{h} - 2\frac{\triangle^+\phi_i}{h} + \frac{\triangle^+\phi_{i+1}}{h}\right)^2 \\
&\quad + \frac{1421461}{1310400}\left(\frac{\triangle^+\phi_{i-3}}{h} + 4\frac{\triangle^+\phi_{i-2}}{h} + 6\frac{\triangle^+\phi_{i-1}}{h} - 4\frac{\triangle^+\phi_i}{h} + \frac{\triangle^+\phi_{i+1}}{h}\right)^2 \\
&= h^2(\phi_i'')^2 - h^3(\phi_i'')(\phi_i''') + O(h^4),
\end{aligned} \tag{2.18}$$

$$\beta_2^- = \left(\frac{\triangle^+\phi_{i-2}}{h} - \frac{\triangle^+\phi_{i-1}}{h}\right)^2 = h^2(\phi_i'')^2 - 2h^3(\phi_i'')(\phi_i''') + O(h^4), \tag{2.19}$$

$$\beta_3^- = \left(\frac{\triangle^+\phi_{i-1}}{h} - \frac{\triangle^+\phi_i}{h}\right)^2 = h^2(\phi_i'')^2 + \frac{h^4}{6}(\phi_i'')(\phi_i^{(4)}) + O(h^6), \tag{2.20}$$

$$\begin{aligned}
\beta_1^+ &= \frac{1}{144}\left(\frac{\triangle^+\phi_{i-2}}{h} - 8\frac{\triangle^+\phi_{i-1}}{h} + 8\frac{\triangle^+\phi_{i+1}}{h} - \frac{\triangle^+\phi_{i+2}}{h}\right)^2 \\
&\quad + \frac{1}{15600}\left(-11\frac{\triangle^+\phi_{i-2}}{h} + 174\frac{\triangle^+\phi_{i-1}}{h} - 326\frac{\triangle^+\phi_i}{h} + 174\frac{\triangle^+\phi_{i+1}}{h} - 11\frac{\triangle^+\phi_{i+2}}{h}\right)^2
\end{aligned}$$

$$+\frac{781}{2880}\left(-\frac{\triangle^+\phi_{i-2}}{h}+2\frac{\triangle^+\phi_{i-1}}{h}-2\frac{\triangle^+\phi_{i+1}}{h}+\frac{\triangle^+\phi_{i+2}}{h}\right)^2$$

$$+\frac{1421461}{1310400}\left(\frac{\triangle^+\phi_{i-2}}{h}-4\frac{\triangle^+\phi_{i-1}}{h}+6\frac{\triangle^+\phi_i}{h}-4\frac{\triangle^+\phi_{i+1}}{h}+\frac{\triangle^+\phi_{i+2}}{h}\right)^2$$

$$=h^2(\phi_i'')^2+h^3(\phi_i'')(\phi_i''')+O(h^4), \tag{2.21}$$

$$\beta_2^+=\left(\frac{\triangle^+\phi_{i-1}}{h}-\frac{\triangle^+\phi_i}{h}\right)^2=h^2(\phi_i'')^2+\frac{h^4}{6}(\phi_i'')(\phi_i^{(4)})+O(h^6), \tag{2.22}$$

$$\beta_3^+=\left(\frac{\triangle^+\phi_i}{h}-\frac{\triangle^+\phi_{i+1}}{h}\right)^2=h^2(\phi_i'')^2+2h^3(\phi_i'')(\phi_i^{(3)})+O(h^4), \tag{2.23}$$

Step 4. We compute the nonlinear weights based on the linear weights and the smoothness indicators. For instance, as shown in [23, 24], we use new $\tau^\pm$ which are simply defined as the absolute difference between $\beta_1^\pm$, $\beta_2^\pm$, and $\beta_3^\pm$, and are little different from that specified in [23, 24]. So the associated difference expansions in Taylor series about ϕ_i are

$$\tau^\pm=\left(\frac{|\beta_1^\pm-\beta_2^\pm|+|\beta_1^\pm-\beta_3^\pm|}{2}\right)^2=O(h^6). \tag{2.24}$$

$$\omega_n^\pm=\frac{\overline{\omega}_n^\pm}{\sum_{\ell=1}^3\overline{\omega}_\ell^\pm},\qquad \overline{\omega}_n=\gamma_n\left(1+\frac{\tau^\pm}{\varepsilon+\beta_n^\pm}\right),\quad n=1,2,3. \tag{2.25}$$

Here ε is a small positive number to avoid the denominator to become zero. It is directly to verify from (2.18) to (2.23) and the parameters $\tau^\pm$, at the smooth regions of the numerical solution satisfying

$$\frac{\tau^\pm}{\varepsilon+\beta_n^\pm}=O(h^4), n=1,2,3, \tag{2.26}$$

on condition that $\varepsilon\ll\beta_n^\pm$. Therefore, the nonlinear weights $\omega_n^\pm$ satisfy the order accuracy condition $\omega_n^\pm=\gamma_n+O(h^4)$ [23, 24], providing the formal fifth-order accuracy to the WENO scheme in [7], 28, [29]. We take $\varepsilon=10^{-6}$ in our computation.

Step 5. The final nonlinear WENO reconstructions $\phi_{x,i}^\pm$ are defined by a convex combination of the three (modified) reconstructed polynomial approximations.

$$\phi_{x,i}^\pm=\omega_1^\pm\left(\frac{1}{\gamma_1}\phi_{x,i}^{\pm,1}-\frac{\gamma_2}{\gamma_1}\phi_{x,i}^{\pm,2}-\frac{\gamma_3}{\gamma_1}\phi_{x,i}^{\pm,3}\right)+\omega_2^\pm\phi_{x,i}^{\pm,2}+\omega_3^\pm\phi_{x,i}^{\pm,3}. \tag{2.27}$$

The terms on the right-hand side of (2.27) are very sophisticated than the usual definition $\omega_1^\pm\phi_{x,i}^{\pm,1}+\omega_2^\pm\phi_{x,i}^{\pm,2}+\omega_3^\pm\phi_{x,i}^{\pm,3}$ which would degrade the optimal fifth-order accuracy because of $\phi_{x,i}^{\pm,2}$ and $\phi_{x,i}^{\pm,3}$ are active and the convex combination together with $\phi_{x,i}^{\pm,1}$ would not offer high order approximation at point x_i to numerical flux in smooth region. Thus we should abolish their contribution in smooth region. By doing such procedure, if a big spatial stencil permits optimal stability and accuracy to be reached, (2.27) could obtain that stability and accuracy obviously. Nevertheless, when the solution on the big spatial stencil is rough, it is beneficial to search for two smaller three-point stencils. Such two small spatial stencils that are used ensure that (when the large six-point spatial stencil may be inoperative). In this way, it is not very essential for us

to deliberately choose linear weights for the purpose of obtaining high-order accuracy in smooth region and could keep high resolutions for the singularities of the derivatives in nonsmooth region.

Step 6. The ODE (2.2) is rewritten as the formula

$$\frac{d\phi_i(t)}{dt} = L(\phi_i). \tag{2.28}$$

Then we use third order version TVD Runge-Kutta time discretization method [30]:

$$\begin{cases} \phi^{(1)} = \phi^n + \triangle t L(\phi^n), \\ \phi^{(2)} = \frac{3}{4}\phi^n + \frac{1}{4}\phi^{(1)} + \frac{1}{4} \triangle t L(\phi^{(1)}), \\ \phi^{n+1} = \frac{1}{3}\phi^n + \frac{2}{3}\phi^{(2)} + \frac{2}{3} \triangle t L(\phi^{(2)}), \end{cases} \tag{2.29}$$

to obtain fully discrete scheme both in space and time.

B. The Framework for Two-Dimensional Case

We take the control Eq. (1.1) in two dimensions. For simplicity, we also assume Ω has been divided as an uniform mesh with intervals $I_{i,j} = [x_{i-1/2}, x_{i+1/2}] \times [y_{j-1/2}, y_{j+1/2}]$, $i = 1, \ldots, N$, $j = 1, \ldots, M$. We denote $(x_i, y_j) = (\frac{1}{2}(x_{i-1/2} + x_{i+1/2}), \frac{1}{2}(y_{j-1/2} + y_{j+1/2}))$, $|I_{i,j}| = (x_{i+1/2} - x_{i-1/2})(y_{j+1/2} - y_{j-1/2}) = h^2$ to be the interval center and the area of $I_{i,j}$, respectively. Then (1.1) can be reformulated as:

$$\begin{cases} \phi_t + H(x, y, t, \phi, \phi_x, \phi_y) = 0, \\ \phi(x, y, 0) = \phi_0(x, y). \end{cases} \tag{2.30}$$

We define $\phi_{i,j} = \phi(x_i, y_j)$, $\triangle_x^+ \phi_{i,j} = \phi_{i+1,j} - \phi_{i,j}$ and $\triangle_y^+ \phi_{i,j} = \phi_{i,j+1} - \phi_{i,j}$. The semidiscrete form in two dimensions is

$$\frac{d\phi_{i,j}(t)}{dt} = L(\phi_{i,j}) = -\hat{H}(x_i, y_j, t, \phi_{i,j}, \phi^+_{x,i,j}, \phi^-_{x,i,j}, \phi^+_{y,i,j}, \phi^-_{y,i,j}). \tag{2.31}$$

where $\hat{H}$ is a Lipschitz continuous monotone flux consistent with H, in the sense that $\hat{H}(x, y, t, \phi, \phi_x, \phi_x, \phi_y, \phi_y) = H(x, y, t, \phi, \phi_x, \phi_y)$. The Lax-Friedrichs flux is applied here:

$$\hat{H}(x, y, t, \phi, u^+, u^-, v^+, v^-) = H\left(x, y, t, \phi, \frac{u^+ + u^-}{2}, \frac{v^+ + v^-}{2}\right) - \alpha \frac{u^+ - u^-}{2} - \beta \frac{v^+ - v^-}{2}, \tag{2.32}$$

where $\alpha = \max_u H_1(u, v)$ and $\beta = \max_v H_2(u, v)$. H_1 stands for the partial derivative of H with respect to ϕ_x and H_2 stands for the partial derivative of H with respect to ϕ_y. Here $\phi^{\pm}_{x,i,j}$ are WENO approximations to $\frac{\partial \phi(x_i, y_j)}{\partial x}$, and $\phi^{\pm}_{y,i,j}$ are WENO approximations to $\frac{\partial \phi(x_i, y_j)}{\partial y}$, which are similar to one-dimensional approximations (2.27). The approximation procedures of $\phi^{\pm}_{x,i,j}$ and $\phi^{\pm}_{y,i,j}$ use a dimension-by-dimension fashion with fixed subscript j and i, respectively.

TABLE I. $\phi_t + \phi_x = 0$. $\phi(x,0) = -\cos(\pi x)$. Periodic boundary conditions. $t = 2$..

Grid points	L^1 error	Order	L^∞ error	Order	L^1 error	Order	L^∞ error	Order
	WENO-ZQ (1) scheme				WENO-JP scheme			
10	1.49 E−2		1.95 E−2		2.71 E−2		4.63 E−2	
20	5.35 E−4	4.80	1.22 E−3	4.00	1.11 E−3	4.59	2.31 E−3	4.32
40	8.62 E−6	5.96	1.48 E−5	6.36	4.06 E−5	4.78	7.09 E−5	5.02
80	2.13 E−7	5.33	3.29 E−7	5.50	1.35 E−6	4.90	2.21 E−6	5.00
160	6.57 E−9	5.02	1.03 E−8	5.00	4.34 E−8	4.96	6.90 E−8	5.00
320	2.05 E−10	5.00	3.22 E−10	5.00	1.36 E−9	4.99	2.15 E−9	5.00
	WENO-ZQ (2) scheme				WENO-ZQ (3) scheme			
10	2.35 E−1		3.38 E−1		2.47 E−1		3.56 E−1	
20	2.18 E−2	3.43	4.27 E−2	2.98	2.43 E−2	3.34	4.63 E−2	2.94
40	4.05 E−4	5.75	2.23 E−3	4.26	7.08 E−4	5.10	3.58 E−3	3.69
80	1.68 E−6	7.91	1.45 E−5	7.26	2.36 E−6	8.22	2.10 E−5	7.41
160	1.07 E−8	7.29	5.38 E−8	8.07	1.27 E−8	7.54	7.97 E−8	8.04
320	2.27 E−10	5.56	3.22 E−10	7.38	2.37 E−10	5.74	3.55 E−10	7.80

III. NUMERICAL TESTS

In this section, we set CFL number to be 0.6 and present the results of numerical tests of the new finite difference WENO scheme as WENO-ZQ which is specified in the previous section both in one and two dimensions, and classical finite difference WENO scheme as WENO-JP which is specified in [7]. For the purpose of testing whether the random choice of the linear weights would pollute the optimal fifth-order accuracy of WENO-ZQ scheme or not, we set different type of linear weights in the numerical accuracy cases as: (1) γ_1=0.998, γ_2=0.001, and γ_3=0.001; (2) γ_1=1.0/3.0, γ_2=1.0/3.0, and γ_3=1.0/3.0; (3) γ_1=0.01, γ_2=0.495, and γ_3=0.495. And set γ_1=0.998, γ_2=0.001, and γ_3=0.001 in the other examples.

Example 3.1. We solve the following linear equation:

$$\phi_t + \phi_x = 0, \ -1 < x < 1, \tag{3.1}$$

with the initial condition $\phi(x,0) = -\cos(\pi x)$ and periodic boundary conditions. When $t = 2$ the solution is still smooth. The errors and numerical orders of accuracy are shown in Table I. We can see the WENO-ZQ achieves its designed order of accuracy in one dimension and sustains less absolute quantity of L^1 and L^∞ errors. We can see that the WENO-ZQ scheme with different type of linear weights achieves close to its designed order of accuracy. And the Fig. 1 shows that WENO-ZQ scheme needs less CPU time than WENO-JP scheme does to obtain the same quantities of L^1 and L^∞ errors.

Example 3.2. We solve the following nonlinear scalar one-dimensional Hamilton-Jacobi equation:

$$\phi_t - \cos(\phi_x + 1) = 0, \ -1 < x < 1, \tag{3.2}$$

with the initial condition $\phi(x,0) = -\cos(\pi x)$ and periodic boundary conditions. We compute the result up to $t = 0.5/\pi^2$. The errors and numerical orders of accuracy are shown in Table II. Again, we can see WENO-ZQ achieves its designed order of accuracy in one dimension. For comparison, errors and numerical orders of accuracy by the classical WENO-JP scheme are shown in

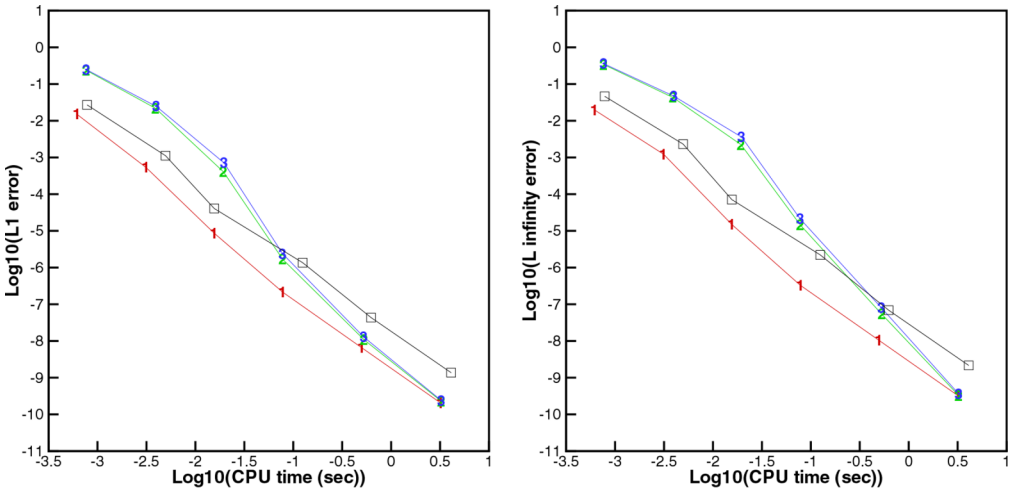

FIG. 1. $\phi_t + \phi_x = 0$. $\phi(x,0) = -\cos(\pi x)$. Computing time and error. Number signs and a solid line denote the results of WENO-ZQ scheme with different linear weights (1), (2), and (3); squares and a solid line denote the results of WENO-JP scheme. [Color figure can be viewed at wileyonlinelibrary.com.]

TABLE II. $\phi_t - \cos(\phi_x + 1) = 0$. $\phi(x,0) = -\cos(\pi x)$. Periodic boundary conditions. $t = 0.5/\pi^2$.

Grid points	L^1 error	Order	L^∞ error	Order	L^1 error	Order	L^∞ error	Order
	WENO-ZQ (1) scheme				WENO-JP scheme			
10	2.73 E−3		6.55 E−3		1.06 E−3		4.66 E−3	
20	9.65 E−5	4.82	4.15 E−4	3.98	9.80 E−5	3.44	3.25 E−4	3.84
40	8.92 E−6	3.43	6.91 E−5	2.59	1.32 E−5	2.88	1.22 E−4	1.41
80	6.39 E−7	3.80	1.08 E−5	2.67	8.18 E−7	4.02	1.79 E−5	2.77
160	2.74 E−8	4.54	7.14 E−7	3.92	3.48 E−8	4.55	1.12 E−6	4.00
320	9.47 E−10	4.85	2.66 E−8	4.75	1.22 E−9	4.83	4.19 E−8	4.75
	WENO-ZQ (2) scheme				WENO-ZQ (3) scheme			
10	6.61 E−3		1.41 E−2		6.74 E−3		1.42 E−2	
20	2.94 E−4	4.49	1.19 E−3	3.56	3.69 E−4	4.19	1.43 E−3	3.32
40	2.63 E−5	3.48	1.57 E−4	2.92	3.22 E−5	3.52	2.10 E−4	2.76
80	6.91 E−7	5.25	1.08 E−5	3.86	7.20 E−7	5.48	1.08 E−5	4.28
160	2.74 E−8	4.66	7.14 E−7	3.92	2.74 E−8	4.71	7.14 E−7	3.92
320	9.47 E−10	4.85	2.66 E−8	4.75	9.47 E−10	4.86	2.66 E−8	4.75

the same table. We can see that both WENO-ZQ and WENO-JP schemes achieve their designed order of accuracy. Figure 2 shows that WENO-ZQ scheme needs less CPU time than WENO-JP does to obtain the same quantities of L^1 and L^∞ errors, so WENO-ZQ scheme is more efficient than WENO-JP scheme in this test case.

Example 3.3. We solve the following nonlinear scalar two-dimensional Burgers' equation:

$$\phi_t + \frac{(\phi_x + \phi_y + 1)^2}{2} = 0, \ -2 \le x, y < 2, \tag{3.3}$$

with the initial condition $\phi(x, y, 0) = -\cos(\pi(x + y)/2)$ and periodic boundary conditions. We compute the result to $t = 0.5/\pi^2$ and the solution is still smooth at that time. The errors

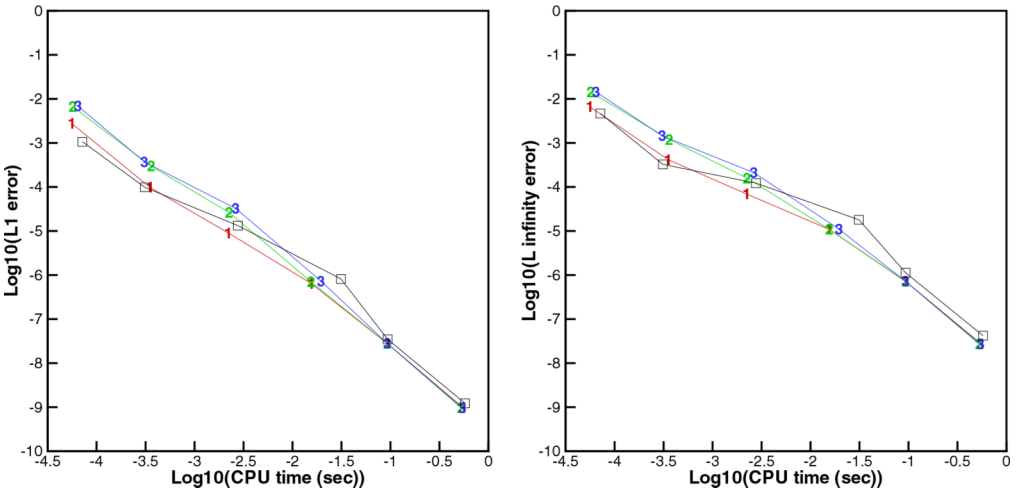

FIG. 2. $\phi_t - \cos(\phi_x + 1) = 0$. $\phi(x, 0) = -\cos(\pi x)$. Computing time and error. Number signs and a solid line denote the results of WENO-ZQ scheme with different linear weights (1), (2), and (3); squares and a solid line denote the results of WENO-JP scheme. [Color figure can be viewed at wileyonlinelibrary.com.]

TABLE III. $\phi_t + \frac{(\phi_x+\phi_y+1)^2}{2} = 0$. $\phi(x, y, 0) = -\cos(\pi(x + y)/2)$. Periodic boundary conditions. $t = 0.5/\pi^2$.

Grid points	L^1 error	Order	L^∞ error	Order	L^1 error	Order	L^∞ error	Order
	WENO-ZQ (1) scheme				WENO-JP scheme			
20×20	1.43 E−4		6.22 E−4		2.70 E−4		1.73 E−3	
40×40	5.91 E−6	4.60	6.57 E−5	3.24	1.35 E−5	4.32	1.55 E−4	3.48
80×80	2.23 E−7	4.73	2.83 E−6	4.54	5.30 E−7	4.67	6.57 E−6	4.56
160×160	7.34 E−9	4.92	9.71 E−8	4.87	1.91 E−8	4.79	2.23 E−7	4.88
320×320	2.34 E−10	4.97	3.10 E−9	4.97	6.63 E−10	4.85	7.12 E−9	4.97
	WENO-ZQ (2) scheme				WENO-ZQ (3) scheme			
20×20	1.13 E−3		4.33 E−3		1.40 E−3		5.00 E−3	
40×40	1.92 E−5	5.88	1.66 E−4	4.70	2.41 E−5	5.87	2.12 E−4	4.56
80×80	2.35 E−7	6.35	2.83 E−6	5.88	2.45 E−7	6.62	2.83 E−6	6.23
160×160	7.26 E−9	5.02	9.71 E−8	4.87	7.23 E−9	5.08	9.71 E−8	4.87
320×320	2.33 E−10	4.96	3.10 E−9	4.97	2.33 E−10	4.95	3.10 E−9	4.97

and numerical orders of accuracy by the WENO-ZQ are shown in Table III and the numerical error against CPU time graphs are in Fig. 3. We can observe that the theoretical order is actually achieved and the WENO-ZQ scheme can get better results and is more efficient than WENO-JP scheme in this test case.

Example 3.4. We solve the following nonlinear scalar two-dimensional Hamilton-Jacobi equation:

$$\phi_t - \cos(\phi_x + \phi_y + 1) = 0, \ -2 \le x, y < 2, \tag{3.4}$$

with the initial condition $\phi(x, y, 0) = -\cos(\pi(x + y)/2)$ and periodic boundary conditions. We also compute the result until $t = 0.5/\pi^2$. The errors and numerical orders of accuracy by the WENO-ZQ scheme with different linear weights in comparison with WENO-JP scheme are shown

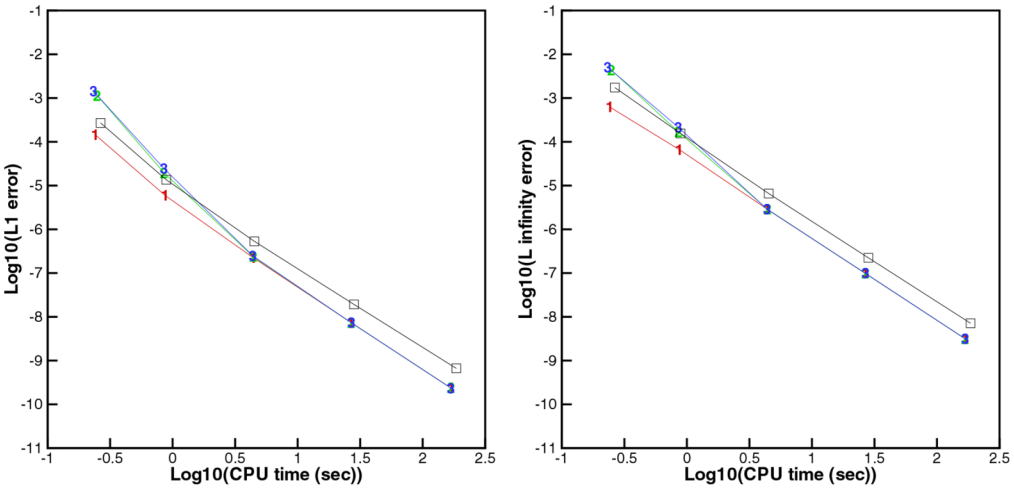

FIG. 3. $\phi_t + \frac{(\phi_x+\phi_y+1)^2}{2} = 0. \phi(x, y, 0) = -\cos(\pi(x+y)/2)$. Computing time and error. Number signs and a solid line denote the results of WENO-ZQ scheme with different linear weights (1), (2), and (3); squares and a solid line denote the results of WENO-JP scheme. [Color figure can be viewed at wileyonlinelibrary.com.]

TABLE IV. $\phi_t - \cos(\phi_x + \phi_y + 1) = 0. \phi(x, y, 0) = -\cos(\pi(x + y)/2)$. Periodic boundary conditions. $t = 0.5/\pi^2$.

Grid points	L^1 error	Order	L^∞ error	Order	L^1 error	Order	L^∞ error	Order
	WENO-ZQ (1) scheme				WENO-JP scheme			
20×20	1.95 E−4		6.75 E−4		2.16 E−4		1.20 E−3	
40×40	1.22 E−5	4.00	1.18 E−4	2.51	1.37 E−5	3.98	1.98 E−4	2.60
80×80	6.17 E−7	4.31	1.16 E−5	3.35	8.05 E−7	4.09	1.88 E−5	3.40
160×160	2.62 E−8	4.56	6.30 E−7	4.21	3.52 E−8	4.51	1.00 E−6	4.22
320×320	9.33 E−10	4.81	2.74 E−8	4.52	1.23 E−9	4.83	4.31 E−8	4.54
	WENO-ZQ (2) scheme				WENO-ZQ (3) scheme			
20×20	5.46 E−4		1.99 E−3		6.15 E−4		2.19 E−3	
40×40	1.38 E−5	5.30	1.19 E−4	4.06	1.45 E−5	5.40	1.19 E−4	4.19
80×80	6.19 E−7	4.48	1.16 E−5	3.36	6.21 E−7	4.55	1.16 E−5	3.37
160×160	2.62 E−8	4.56	6.30 E−7	4.21	2.62 E−8	4.57	6.30 E−7	4.21
320×320	9.33 E−10	4.81	2.74 E−8	4.52	9.33 E−10	4.81	2.74 E−8	4.52

in Table IV and the numerical error against CPU time graphs are in Fig. 4. WENO-ZQ scheme with different type of linear weights is better than WENO-JP scheme in this two-dimensional test case.

Example 3.5. We solve the linear equation:

$$\phi_t + \phi_x = 0, \tag{3.5}$$

with the initial condition $\phi(x, 0) = \phi_0(x - 0.5)$ together with the periodic boundary conditions, where:

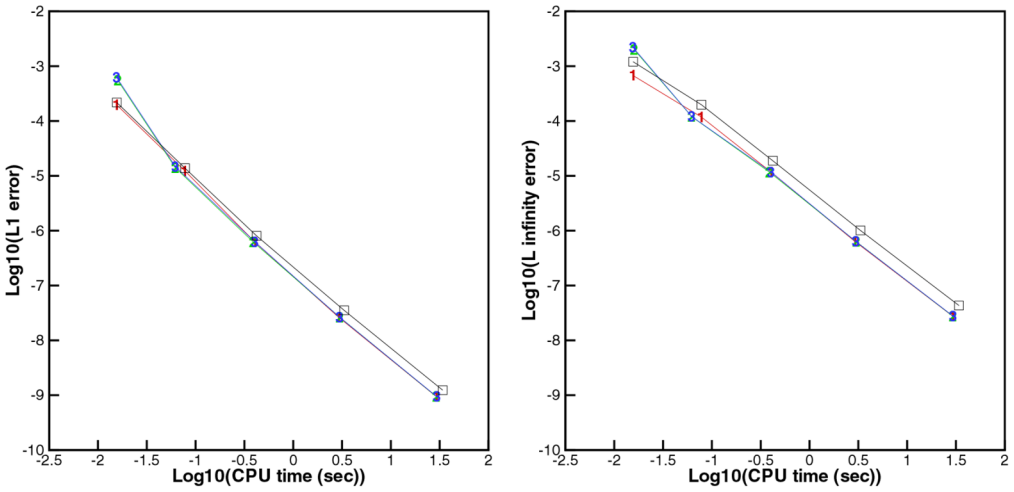

FIG. 4. $\phi_t - \cos(\phi_x + \phi_y + 1) = 0$. $\phi(x, y, 0) = -\cos(\pi(x + y)/2)$. Computing time and error. Number signs and a solid line denote the results of WENO-ZQ scheme with different linear weights (1), (2), and (3); squares and a solid line denote the results of WENO-JP scheme. [Color figure can be viewed at wileyonlinelibrary.com.]

$$\phi_0(x) = -\left(\frac{\sqrt{3}}{2} + \frac{9}{2} + \frac{2\pi}{3}\right)(x+1) + \begin{cases} 2\cos\left(\frac{3\pi x^2}{2}\right) - \sqrt{3}, & -1 \le x < -\frac{1}{3}, \\ \frac{3}{2} + 3\cos(2\pi x), & -\frac{1}{3} \le x < 0, \\ \frac{15}{2} - 3\cos(2\pi x), & 0 \le x < \frac{1}{3}, \\ \frac{28+4\pi+\cos(3\pi x)}{3} + 6\pi x(x-1), & \frac{1}{3} \le x < 1. \end{cases} \tag{3.6}$$

We plot the results with 100 cells at $t = 2$ and $t = 8$ in Fig. 5. We can observe that the results by the WENO-ZQ have good resolution for the corner singularity.

Example 3.6. We solve the one-dimensional nonlinear Burgers' equation:

$$\phi_t + \frac{(\phi_x + 1)^2}{2} = 0, \tag{3.7}$$

with the initial condition $\phi(x, 0) = -\cos(\pi x)$ and the periodic boundary conditions. We plot the results at $t = 3.5/\pi^2$ when discontinuous derivative appears. The solutions of the WENO-ZQ are given in Fig. 6. We can see the scheme gives good results for this problem.

Example 3.7. We solve the nonlinear equation with a non-convex flux:

$$\phi_t - cos(\phi_x + 1) = 0, \tag{3.8}$$

with the initial data $\phi(x, 0) = -\cos(\pi x)$ and the periodic boundary conditions. Then we plot the results at $t = 1.5/\pi^2$ in Fig. 7 when the discontinuous derivative appears in the solution. We can see that the WENO-ZQ gives good results for this problem.

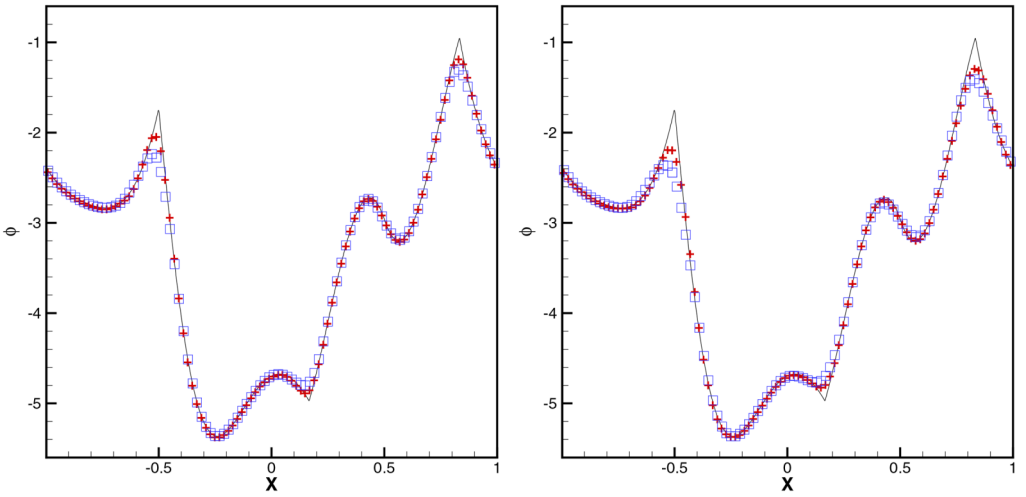

FIG. 5. One dimensional linear equation. 100 grid points. Left: $t = 2$; right: $t = 8$. Solid line: the exact solution; cross symbols: WENO-ZQ scheme; square symbols: WENO-JP scheme. [Color figure can be viewed at wileyonlinelibrary.com.]

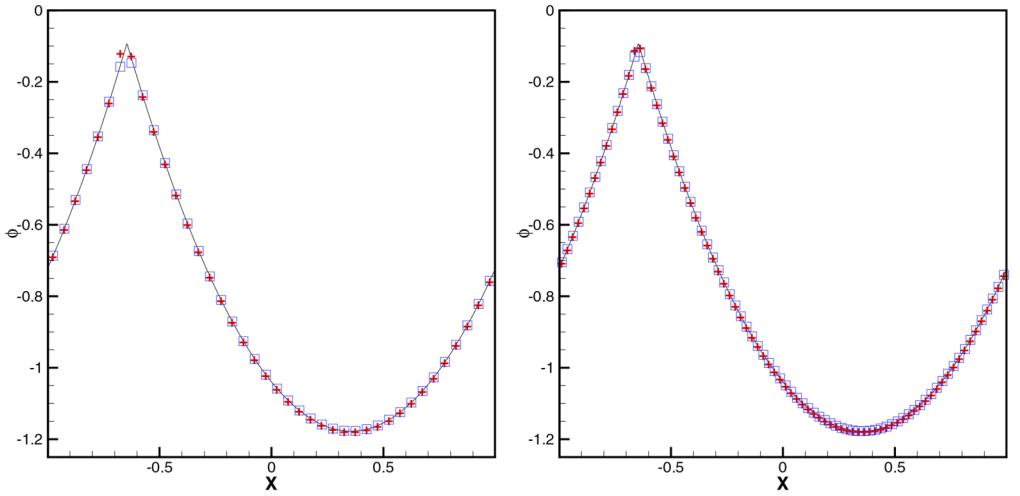

FIG. 6. One dimensional Burgers' equation. Left: 40 grid points; right: 80 grid points. $t = 3.5/\pi^2$. Solid line: the exact solution; cross symbols: WENO-ZQ scheme; square symbols: WENO-JP scheme. [Color figure can be viewed at wileyonlinelibrary.com.]

Example 3.8. We solve the one-dimensional Riemann problem with a non-convex flux:

$$\begin{cases} \phi_t + \frac{1}{4}(\phi_x^2 - 1)(\phi_x^2 - 4) = 0, \ -1 < x < 1, \\ \phi(x, 0) = -2|x|. \end{cases} \tag{3.9}$$

This is a demanding test case, for many schemes have poor resolutions or could even converge to a non-viscosity solution for this case. We plot the results at $t = 1$ by the scheme with 80 grid points to verify the numerical solution in Fig. 8. We can see that such scheme gives good results for this problem.

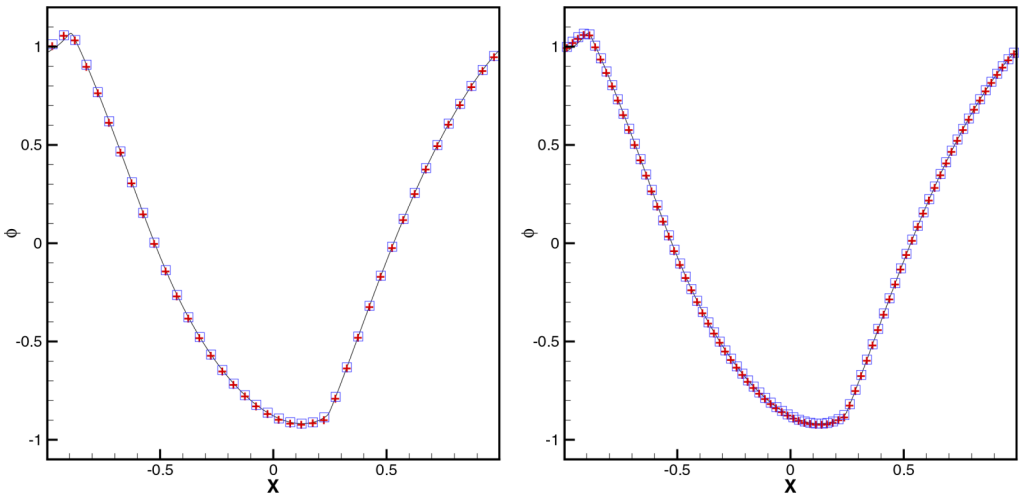

FIG. 7. Problem with the non-convex flux $H(\phi_x) = -\cos(\phi_x + 1)$. Left: 40 cells; right: 80 grid points. $t = 3.5/\pi^2$. Solid line: the exact solution; cross symbols: WENO-ZQ scheme; square symbols: WENO-JP scheme. [Color figure can be viewed at wileyonlinelibrary.com.]

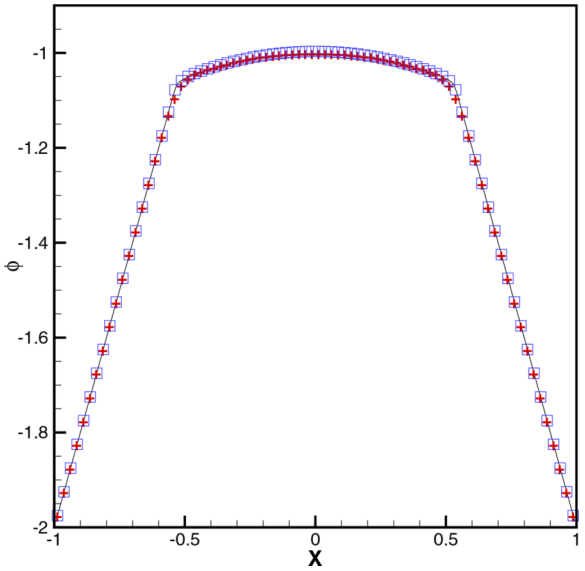

FIG. 8. Problem with the non-convex flux $H(\phi_x) = \frac{1}{4}(\phi_x^2 - 1)(\phi_x^2 - 4)$. 80 grid points. $t = 1$. Solid line: the exact solution; cross symbols: WENO-ZQ scheme; square symbols: WENO-JP scheme. [Color figure can be viewed at wileyonlinelibrary.com.]

Example 3.9. We solve the same two-dimensional nonlinear Burgers' Eq. (3.3) as in Example 3.3 with the same initial condition $\phi(x, y, 0) = -\cos(\pi(x + y)/2)$, except that we now plot the results at $t = 1.5/\pi^2$ in Fig. 9 when the discontinuous derivative has already appeared in the solution. We observe good resolutions for this example.

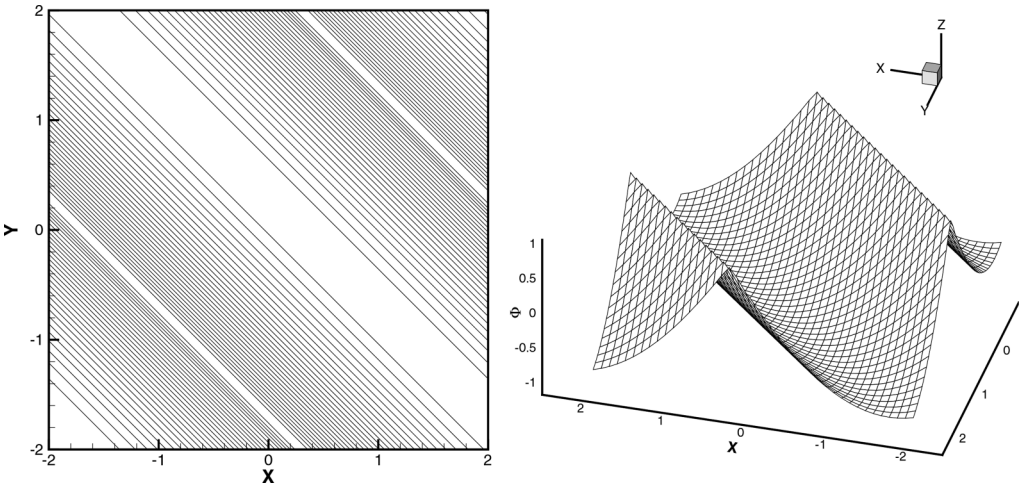

FIG. 9. Two dimensional Burgers' equation. 40×40 grid points. $t = 1.5/\pi^2$. WENO-ZQ scheme. Left: contours of the solution; right: the surface of the solution.

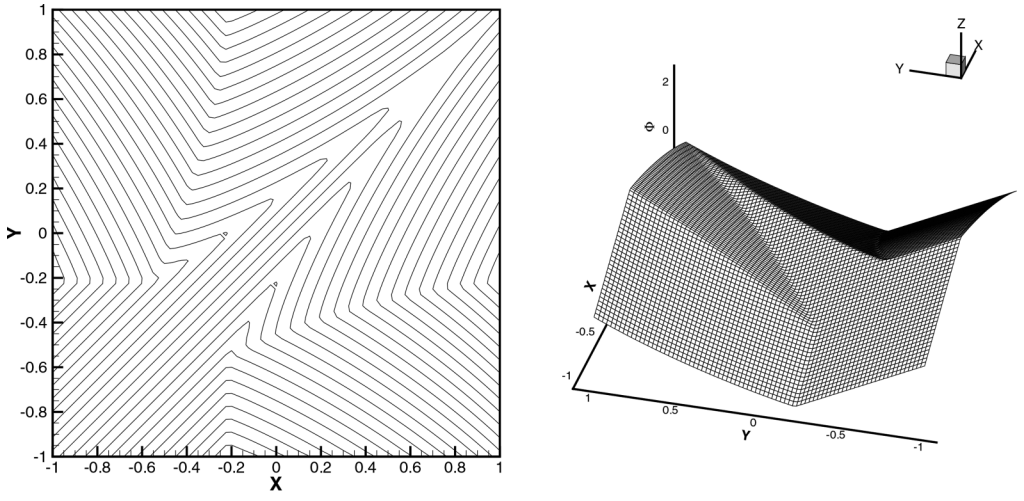

FIG. 10. Two dimensional Riemann problem with a non-convex flux $H(\phi_x, \phi_y) = \sin(\phi_x + \phi_y)$. 80×80 grid points. $t = 1$. WENO-ZQ scheme. Left: contours of the solution; right: the surface of the solution.

Example 3.10. *The two-dimensional Riemann problem with a non-convex flux:*

$$\begin{cases} \phi_t + \sin(\phi_x + \phi_y) = 0, \ -1 \le x, y < 1, \\ \phi(x, y, 0) = \pi(|y| - |x|). \end{cases} \tag{3.10}$$

The solution of the WENO-ZQ is plotted at $t = 1$ in Fig. 10. We can also observe good resolutions for this numerical simulation.

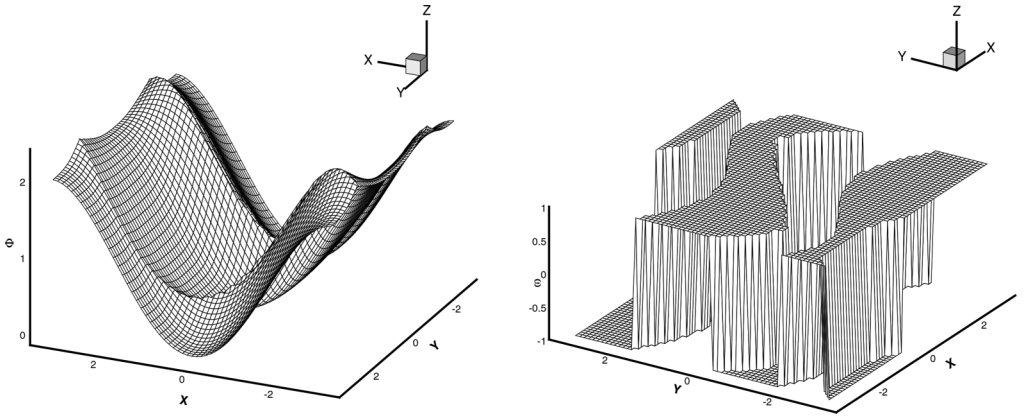

FIG. 11. The optimal control problem. 60×60 grid points. $t = 1$. WENO-ZQ scheme. Left: the surface of the solution; right: the optimal control $\omega = \text{sign}\,(\phi_y)$.

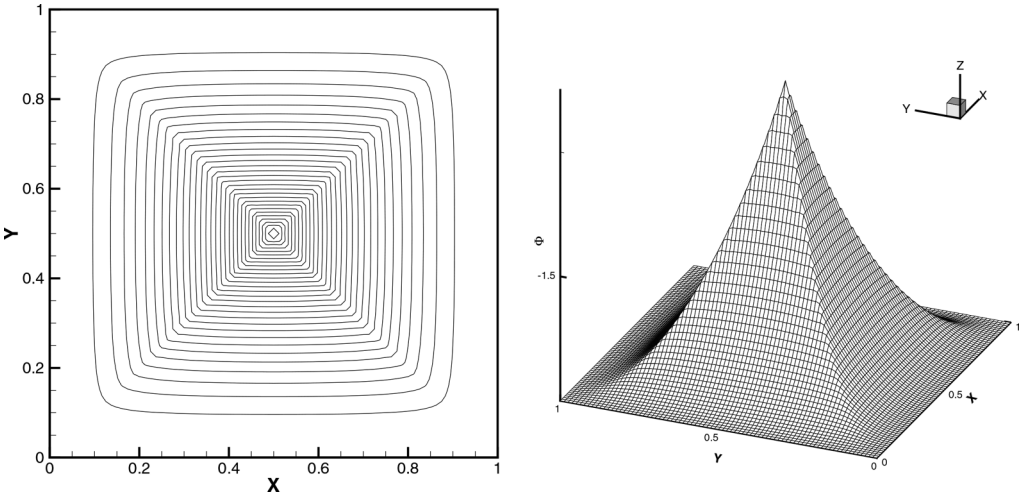

FIG. 12. Eikonal equation with a non-convex Hamiltonian. 80×80 grid points. $t = 0.6$. WENO-ZQ scheme. Left: contours of the solution; right: the surface of the solution.

Example 3.11. A problem from optimal control:

$$\begin{cases} \phi_t + \sin(y)\phi_x + (\sin(x) + sign(\phi_y))\phi_y - \frac{1}{2}\sin(y)^2 - (1 - \cos(x)) = 0, \quad \pi \le x, y < \pi, \\ \phi(x, y, 0) = 0, \end{cases} \tag{3.11}$$

with periodic conditions, see [6]. The solutions of WENO-ZQ are plotted at $t = 1$ and the optimal control $\omega = \text{sign}\,(\phi_y)$ is shown in Fig. 11.

Example 3.12. A two-dimensional Eikonal equation with a non-convex Hamiltonian, which arises in geometric optics [31], is given by:

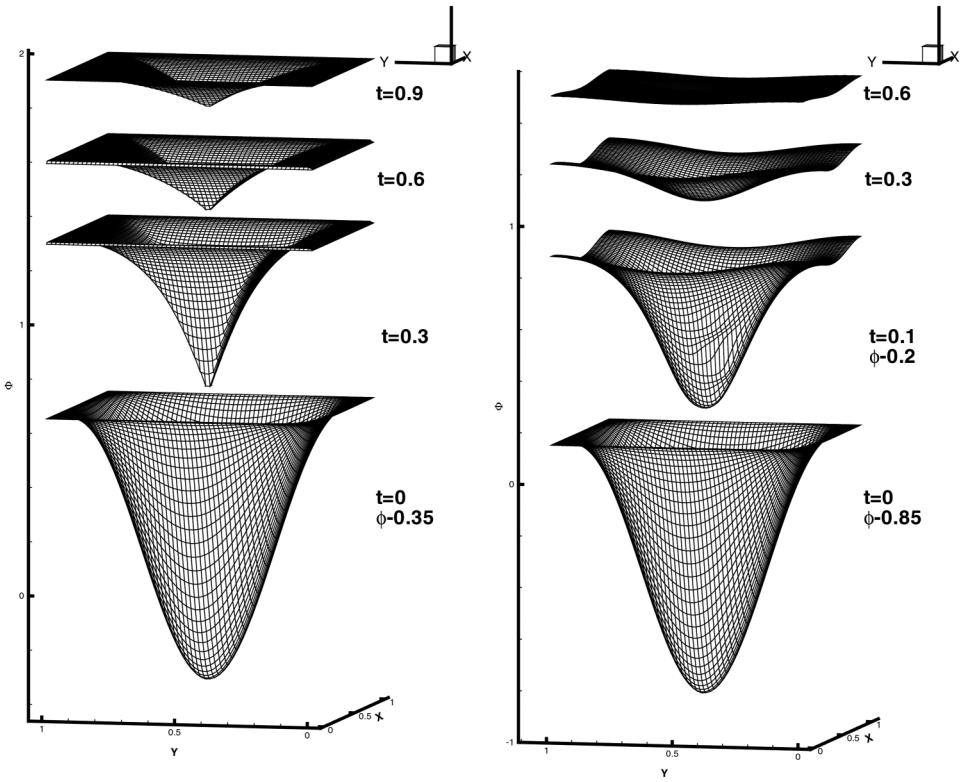

FIG. 13. Propagating surface. 60×60 grid points. Left: $\varepsilon = 0$; right: $\varepsilon = 0.1$. WENO-ZQ scheme.

$$\begin{cases} \phi_t + \sqrt{\phi_x^2 + \phi_y^2 + 1} = 0, \quad 0 \le x, y < 1, \\ \phi(x, y, 0) = \frac{1}{4}(\cos(2\pi x) - 1)(\cos(2\pi y) - 1) - 1, \end{cases} \tag{3.12}$$

The solutions of the WENO-ZQ are plotted at $t = 0.6$ in Fig. 12. Good resolutions are observed with the proposed scheme.

Example 3.13. The problem of a propagating surface [5]:

$$\begin{cases} \phi_t - (1 - \varepsilon K)\sqrt{\phi_x^2 + \phi_y^2 + 1} = 0, \quad 0 \le x, y < 1, \\ \phi(x, y, 0) = 1 - \frac{1}{4}(\cos(2\pi x) - 1)(\cos(2\pi y) - 1), \end{cases} \tag{3.13}$$

where K is the mean curvature defined by:

$$K = -\frac{\phi_{xx}(1 + \phi_y)^2 - 2\phi_{xy}\phi_x\phi_y + \phi_{yy}(1 + \phi_x^2)}{(1 + \phi_x^2 + \phi_y^2)^{3/2}},$$

and ε is a small constant. Periodic boundary conditions are used. The approximation of K is constructed by the methods similar to the first derivative terms and three different second order derivatives of associated Hermite reconstruction polynomials are needed. The results of $\varepsilon = 0$

(pure convection) and $\varepsilon = 0.1$ by WENO-ZQ are presented in Fig. 13. The surfaces at $t = 0$ for $\varepsilon = 0$ and for $\varepsilon = 0.1$, and at $t = 0.1$ for $\varepsilon = 0.1$, are shifted downward to show the detail of the solution at later time.

IV. CONCLUDING REMARKS

In this paper, we have constructed a new fifth order finite difference WENO scheme which is a WENO type combination of a modified fifth order scheme and two second order schemes for solving the Hamilton-Jacobi equations in one and two dimensions. The main advantages of such methodology are its simplicity in spatial field by the definition of positive linear weights, and only one six-point stencil and two three-point stencils are needed on constructing different polynomials. Therefore, we try to use central scheme in smooth regions for simplicity and obtain high order numerical accuracy, and switch to either of two lower order schemes when adjacent discontinuities for the purpose of avoiding spurious oscillations. For the sake of confining the new WENO scheme converge to the optimal fifth-order accuracy in smooth regions, we modify the fourth degree polynomial by subtracting two parameterized linear polynomials. Thereafter, new nonlinear weight's formulas are presented for these polynomials of different degrees based on the information that defined on these unequal spatial stencils. Generally speaking, the constructions of such new WENO scheme are based on WENO interpolation in spatial field and then Runge-Kutta discretization is used for solving the ODE. In the new WENO scheme, the nodal point information is used via time approaching and is easier to be implemented than the classical finite difference WENO scheme. This scheme sustains high-order accuracy in the smooth regions and obtains high resolutions for the singularities of the derivatives robustly. Extensive numerical experiments are performed to illustrate the effectiveness of the new WENO scheme.

References

1. C. K. Chan, K. S. Lau, and B. L. Zhang, Simulation of a premixed turbulent Name with the discrete vortex method, Int J Numer Methods Eng 48 (2000), 613–627.
2. P. L. Lions, Generalized solutions of Hamilton-Jacobi equations, Pitman, London, 1982.
3. J. A. Sethian, Level set methods and fast marching methods, evolving interface, computational geometry, fluid mechanics, computer vision, and materials science, Cambridge University Press, Cambridge, 1999.
4. R. Abgrall and T. Sonar, On the use of Muehlbach expansions in the recovery step of ENO methods, Numer Math, 76 (1997), 1–25.
5. S. Osher and J. Sethian, Fronts propagating with curvature dependent speed: Algorithms based on Hamilton-Jacobi formulations, J Comput Phys 79 (1988), 12–49.
6. S. Osher and C.-W. Shu, High-order essentially nonoscillatory schemes for Hamilton-Jacobi equations, SIAM J Numer Anal 28 (1991), 907–922.
7. G. S. Jiang and D. Peng, Weighted ENO schemes for Hamilton-Jacobi equations, SIAM J Sci Comput 21 (2000), 2126–2143.
8. J. Qiu, WENO schemes with Lax-Wendroff type time discretizations for Hamilton-Jacobi equations, J Comput Appl Math 200 (2007), 591–605.
9. J. Qiu, Hermite WENO schemes with Lax-Wendroff type time discretizations for Hamilton-Jacobi equations, J Comput Math 25 (2007), 131–144.
10. J. Qiu and C.-W. Shu, Hermite WENO schemes for Hamilton-Jacobi equations, J Comput Phys 204 (2005), 82–99.

11. F. Lafon and S. Osher, High order two dimensional nonoscillatory methods for solving Hamilton-Jacobi scalar equations, J Comput Phys 123 (1996), 235–253.

12. Y. T. Zhang and C.-W. Shu, High-order WENO schemes for Hamilton-Jacobi equations on triangular meshes, SIAM J Sci Comput 24 (2003), 1005–1030.

13. X. G. Li and C. K. Chan, High-order schemes for Hamilton-Jacobi equations on triangular meshes, J Comput Appl Math 167 (2004), 227–241.

14. S. Augoula and R. Abgrall, High order numerical discretization for Hamilton-Jacobi equations on triangular meshes, J Sci Comput 15 (2000), 198–229.

15. T. J. Barth and J. A. Sethian, Numerical schemes for the Hamilton-Jacobi and level set equations on triangulated domains, J Comput Phys 145 (1998), 1–40.

16. C. Hu and C.-W. Shu, A discontinuous Galerkin finite element method for Hamilton-Jacobi equations, SIAM J Sci Comput 21 (1999), 666–690.

17. O. Lepsky, C. Hu, and C.-W. Shu, Analysis of the discontinuous Galerkin method for Hamilton-Jacobi equations, Appl Numer Math 33 (2000), 423–434.

18. Y. D. Cheng and C.-W. Shu, A discontinuous Galerkin finite element method for directly solving the Hamilton-Jacobi equations, J Comput Phys 223 (2007), 398–415.

19. J. Yan and S. Osher, A local discontinuous Galerkin method for directly solving Hamilton-Jacobi equations, J Comput Phys 230 (2011), 232–244.

20. J. Qiu and C.-W. Shu, Hermite WENO schemes and their application as limiters for Runge-Kutta discontinuous Galerkin method: one dimensional case, J Comput Phys 193 (2004), 115–135.

21. J. Qiu and C.-W. Shu, Hermite WENO schemes and their application as limiters for Runge-Kutta discontinuous Galerkin method II: two-dimensional case, Comput Fluids 34 (2005), 642–663.

22. J. Zhu and J. Qiu, A new fifth order finite difference WENO scheme for solving hyperbolic conservation laws, J Comput Phys 318 (2016), 110–121.

23. R. Borges, M. Carmona, B. Costa, and W. S. Don, An improved weighted essentially non-oscillatory scheme for hyperbolic conservation laws, J Comput Phys 227 (2008), 3191–3211.

24. M. Castro, B. Costa, and W. S. Don, High order weighted essentially non-oscillatory WENO-Z schemes for hyperbolic conservation laws, J Comput Phys 230 (2011), 1766–1792.

25. J. Zhu and N. Zhao, A kind of MWENO scheme and its applications, Acta Aerodyn Sin, 23 (2005), 330–333,

26. J. Zhu, N. Zhao, and H. S. Zheng, A kind of MWENO spectral volume (SVMWENO5) scheme, Acta Aerodyn Sin, 24 (2006), 331–334, (in Chinese).

27. D. S. Balsara, T. Rumpf, M. Dumbser, and C. D. Munz, Efficient, high accuracy ADER-WENO schemes for hydrodynamics and divergence-free magnetohydrodynamics, J Comput Phys 228 (2009), 2480–2516.

28. G. S. Jiang and C.-W. Shu, Efficient implementation of weighted ENO schemes, J Comput Phys 126 (1996), 202–228.

29. C.-W. Shu, Essentially non-oscillatory and weighted essentially non-oscillatory schemes for hyperbolic conservation laws, B. Cockburn, C. Johnson, C.-W. Shu, and E. Tadmor, A. Quarteroni, editors, Lecture Notes in Mathematics, Vol. 1697, Advanced numerical approximation of nonlinear hyperbolic equations, Springer-Verlag, Berlin, 1998, pp. 325–432.

30. C.-W. Shu and S. Osher, Efficient implementation of essentially non-oscillatory shock capturing schemes, J Comput Phys 77 (1988), 439–471.

31. S. Jin and Z. Xin, Numerical passage from systems of conservation laws to Hamilton-Jacobi equations, and relaxation schemes, SIAM J Numer Anal 35 (1998), 2163–2186.